

1 **Observations of atmospheric $^{14}\text{CO}_2$ at Anmyeondo GAW station,**
2 **Korea: Implications for fossil fuel CO_2 and emission ratios**

3 Haeyoung Lee^{1,2}, Edward J. Dlugokencky³, Jocelyn C Turnbull^{4,5}, Sepyo Lee¹, Scott J. Lehman⁶,
4 John B Miller³, Gabrielle Petron^{3,5}, Jeongsik Lim^{7,8}, and Gang-Woong Lee², Sang-Sam Lee¹ and
5 Young-San Park¹

6

7

8 *Correspondence to Haeyoung Lee (leehy80@korea.kr)*

9

10 ¹National Institute of Meteorological Sciences, Jeju, 63568, Republic of Korea

11 ²Atmospheric Chemistry Laboratory, Hankuk University of Foreign Studies, Gyeonggi-do, 17035, Republic of
12 Korea

13 ³NOAA, Global Monitoring Laboratory, Boulder, Colorado, USA

14 ⁴National Isotope Center, GNS Science, Lower Hutt, New Zealand

15 ⁵CIRES, University of Colorado, Boulder, Colorado, USA

16 ⁶INSTAAR, University of Colorado, Boulder, Colorado, USA

17 ⁷Korea Research Institute of Standard and Science, Daejeon, 34113, Republic of Korea

18 ⁸University of Science and Technology, Daejeon, 34113, Republic of Korea

19 *Abstract. To understand Korea's carbon dioxide (CO_2) emissions and sinks as well as those of*
20 *the surrounding region, we used 70 flask-air samples collected during May 2014 to August 2016*
21 *at Anmyeondo (AMY, 36.53°N , 126.32°E ; 46 m a.s.l) World Meteorological Organization*
22 *(WMO) Global Atmosphere Watch (GAW) station, located on the west coast of South Korea, for*
23 *analysis of observed ^{14}C in atmospheric CO_2 as a tracer of fossil fuel CO_2 contribution (C_{ff}).*

24 *Observed $^{14}\text{C/C}$ ratios in CO_2 (reported as Δ values) at AMY varied from -59.5 to 23.1‰ with a*
25 *measurement uncertainty of $\pm 1.8\%$. The derived mean value C_{ff} of $(9.7 \pm 7.8) \mu\text{mol mol}^{-1}$ (1σ) is*
26 *greater than that found in earlier observations from Tae-Ahn Peninsula (TAP, 36.73°N , 126.13°*
27 *E, 20 m a.s.l., 28 km away from AMY) of $(4.4 \pm 5.7) \mu\text{mol mol}^{-1}$ from 2004 to 2010. The*
28 *enhancement above background mole fraction of sulfur hexafluoride ($\Delta x(\text{SF}_6)$) and carbon*
29 *monoxide ($\Delta x(\text{CO})$) correlate strongly with C_{ff} ($r > 0.7$) and appear to be good proxies for fossil*

30 fuel CO_2 at regional and continental scales. Samples originating from the Asian continent had
31 greater $\Delta x(CO):C_{ff}(R_{CO})$ values, (29 ± 8) to (36 ± 2) $nmol \mu mol^{-1}$, than in Korean local air $((8 \pm 2)$
32 $nmol \mu mol^{-1}$). Air masses originating in China showed (1.6 ± 0.4) to (2.0 ± 0.1) times greater R_{CO}
33 than a bottom-up inventory suggesting that China's CO emissions are underestimated in the
34 inventory while observed R_{SF6} values are 2-3 times greater than inventories for both China and
35 Korea. However, both R_{CO} derived from inventories and observations have decreased relative to
36 previous studies, indicating that combustion efficiency is increasing in both China and South
37 Korea.

38 1 Introduction

39 Carbon Dioxide (CO_2) is the principle cause of climate change in the industrial era, and is
40 increasing in the atmosphere at $(2.4 \pm 0.4) \mu mol mol^{-1} a^{-1}$ in a recent decade globally (where 0.4
41 is the standard deviation of annual growth rates; www.esrl.noaa.gov/gmd/ccgg/trends/, last
42 access: 6 December 2019). This increase is by release of CO_2 from fossil fuel combustion that
43 has been demonstrated through ^{14}C analysis of tree rings from the last two centuries (Stuiver and
44 Quay, 1981; Suess, 1955; Tans et al., 1979). Atmospheric measurement program for the ratio
45 $^{14}C/C$ in CO_2 was initiated in the 1950s and 1960s (Rafter and Fergusson, 1957; Nydal, 1996).
46 Observed $^{14}C/C$ ratios are reported in Delta notation ($\Delta(^{14}CO_2)$) as fractionation-corrected permil
47 (or ‰) deviations from the absolute radiocarbon standard (Stuiver and Polach, 1977). Many
48 studies show that the variation of $\Delta(^{14}CO_2)$ is an unbiased and now widely used tracer for CO_2
49 emitted from fossil-fuel combustion (Levin et al., 2003; Turnbull et al., 2006; Graven et al., 2009;

50 Van der Laan et al., 2010; Miller et al., 2012). Therefore measurements of $\Delta(^{14}\text{CO}_2)$ are
51 important to test the effectiveness of emission reduction strategies to mitigate the rapid
52 atmospheric CO₂ increase, since they can partition observed CO₂ enhancements, $\Delta x(\text{CO}_2)$, into
53 fossil fuel CO₂ (C_{ff}) and biological CO₂ (C_{bio}) components with high confidence (Turnbull et al.,
54 2006).

55 When trace gases are co-emitted with C_{ff} , correlations of their enhancements with C_{ff} improve
56 understanding of the emission sources of both C_{ff} and the co-emitted tracers. For example, CO
57 and CH₄ emission inventories are typically more uncertain than the fossil fuel CO₂ emission
58 inventory, since fossil fuel CO₂ emissions related to complete combustion are generally well
59 estimated while emissions related to incomplete combustion and agricultural activities are poorly
60 constrained (Kurokawa et al., 2013). Temporal changes in the observed emission ratio of a trace
61 gas to C_{ff} can be used to examine emission trends in the trace gas (Tohijima et al., 2014).
62 Therefore the observed emission ratios of trace gases to C_{ff} can be used to evaluate bottom-up
63 inventories of various trace gases (e.g., Miller et al., 2012). Here, we used two trace gases,
64 carbon monoxide (CO) and sulfur hexafluoride (SF₆) for this analysis. CO is produced along
65 with CO₂ during incomplete combustion of fossil fuels and biomass. CO enhancements above
66 background ($\Delta x(\text{CO}_2)$) correlate well with C_{ff} and have been used as a fossil fuel tracer
67 (Zondervan and Meijer, 1996; Gamnitzer et al., 2006; Turnbull et al., 2011a; Turnbull et al.,
68 2011b; Tohijima et al., 2014). SF₆ is an entirely anthropogenic gas and is widely used as an arc
69 quencher in high-voltage electrical equipment (Geller et al., 1997). At regional to continental
70 scales, persistent small leaks to the atmosphere of SF₆ are typically co-located with fossil fuel
71 CO₂ sources and allow SF₆ to be used as an indirect C_{ff} tracer, if the leaks are co-located with C_{ff}
72 emissions at the location and scale of interest (Turnbull et al., 2006; Rivier et al., 2006).

73 South Korea is a rapidly developing country with fast economic growth, and it is located next to
74 China, which is the world's largest emitter of anthropogenic CO₂ (Boden et al., 2017; Janssens-
75 Maenhout et al., 2017). The first $\Delta(^{14}\text{CO}_2)$ measurements in South Korea were reported by
76 Turnbull et al. (2011a) based on air samples collected during October 2004 to March 2010 at
77 Tae-Ahn Peninsula (TAP, 36.73° N, 126.13° E, 20 m a.s.l.). This study showed that observed
78 CO₂ at this site was often influenced by Chinese emissions and the observed ratio of $\Delta x(\text{CO}) : C_{\text{ff}}$
79 (R_{CO}) was greater than expected from bottom-up inventories. However South Korean $\Delta(^{14}\text{CO}_2)$
80 data are still limited and the ratio of the other trace gases to C_{ff} barely discussed.

81 Here we use whole-air samples collected in glass flasks during May 2014 to August 2016 at
82 Anmyeondo (AMY, 36.53° N, 126.32° E; 46 m a.s.l.) World Meteorological Organization
83 (WMO) Global Atmosphere Watch (GAW) station, located on the west coast of South Korea and
84 about 28 km SSE of TAP, where the first study was conducted. We decompose observed CO₂
85 enhancements into their fossil fuel and biological components at AMY to understand sources and
86 sinks of CO₂. We also implemented cluster analysis using the NOAA Hybrid Single Particle
87 Lagrangian Integrated Trajectory Model (HYSPLIT) to calculate back-trajectories for sample
88 times and dates. Based on clusters of trajectories from specific regions, trace gas enhancement:
89 C_{ff} ratios and correlation coefficients were analyzed, especially focused on SF₆ and CO, to
90 determine the potential of alternative proxies to $\Delta(^{14}\text{CO}_2)$. Finally we compared our $\Delta x(\text{CO}) : C_{\text{ff}}$
91 ratio with ratios determined from bottom-up inventories (EDGARv4.3.2 and Korea's National
92 Inventory Report in 2018) to evaluate reported CO emissions and how they've changed since
93 2010.

94

95 **2. Materials and Methods**

96 **2.1 Sampling site and methods**

97 The AMY GAW station is managed by the National Institute of Meteorological Sciences (NIMS)
98 in the Korea Meteorological Administration (KMA). It has the longest record of continuous CO₂
99 measurement in South Korea, beginning in 1999. It is located on the west coast of Korea about
100 130 km southwest of the megacity of Seoul, whose population was 9.8 million in 2017.
101 Semiconductor and other industries exist within a 100 km radius of the station. Also, the largest
102 thermal power plants fired by coal and heavy oil in South Korea are within 35 km to the
103 northeast and southeast of the station. The closest town, around 30 km to the east of AMY, is
104 well known for its livestock industries. Local economic activities are related to agriculture, e.g.,
105 production of rice paddies, sweet potatoes, and onions, and the area is also known for its leisure
106 opportunities that increase traffic and tourists in summer, indicating the complexity of
107 greenhouse gas sources around AMY. On the other hand, air masses often arrive at AMY from
108 the west and south, which is open to the Yellow Sea. Therefore AMY observes enhanced CO₂
109 compared to many other East Asian stations due not only to numerous local sources but also
110 long-range transport of air-masses from the Asian continent (Lee et al., 2019).

111 Two pairs of flask-air samples (4 flasks total, 2 L, borosilicate glass with Teflon O-ring sealed
112 stopcocks) were collected about weekly from a 40 m tall tower at AMY, regardless of wind
113 direction and speed from May 2014 to August 2016, generally between 1400 to 1600 local time
114 (Table S1) using a semi-automated portable sampler. A pair of flasks was flushed for 10 min at
115 5-6 L min⁻¹ then pressurized to 0.38 bar in less than 1 min. A second pair is collected shortly
116 after the first (within 20 min). The portable sampler was checked for leaks after pressurizing by

117 observing the pressure gauge before closing the stopcocks. Batches of sampled flasks were
118 shipped to Boulder, CO, USA every two months.

119 A total of 70 sets were collected and analyzed at the National Oceanic and Atmospheric
120 Administration/Earth System Research Laboratory/Global Monitoring Division
121 (NOAA/ESRL/GMD) for CO₂, CO, and SF₆ and for $\Delta(^{14}\text{CO}_2)$ by University of Colorado
122 Boulder, Institute of Arctic and Alpine Research (INSTAAR). NOAA/ESRL/GMD analyzed
123 CO₂ using a non-dispersive infrared analyzer, SF₆ using gas chromatography (GC) with electron
124 capture detection, and CO by vacuum UV, resonance fluorescence. All analyzers were calibrated
125 with the appropriate WMO mole fraction scales (WMO-X2007 scale for CO₂, WMO-X2014A
126 scale for CO, and WMO-X2014 for SF₆; <https://www.esrl.noaa.gov/gmd/ccl/>, last access: 4
127 December 2019). The measurement and analysis methods for those gases are described in detail
128 (http://www.esrl.noaa.gov/gmd/ccgg/behind_the_scenes/measurementlab.html, last access: 4
129 December 2019). Measurement uncertainties for CO₂ and SF₆ are reported as 68% confidential
130 intervals. For CO₂, it is 0.07 $\mu\text{mol mol}^{-1}$ for all measurements used here. For SF₆, it is 0.04 pmol
131 mol^{-1} . For CO, measurement uncertainty has not yet been formally evaluated, but is estimated at
132 1 nmol mol^{-1} (68% confidence interval). All CO₂, SF₆ and CO data at AMY can be downloaded
133 through ftp://aftp.cmdl.noaa.gov/data/trace_gases/. When we compare NOAA's CO₂
134 measurements from flask-air with quasi-continuous measurements by KMA at AMY, the
135 difference was $-0.11 \pm 2.32 \mu\text{mol mol}^{-1}$ (mean $\pm 1 \sigma$), close to GAW's compatibility goal for CO₂
136 (± 0.1 ppm for Northern Hemisphere measurements, Lee et al., 2019).

137 The analysis methods for $\Delta(^{14}\text{CO}_2)$ are described by Lehman et al.(2013). Measurement
138 repeatability of $\Delta(^{14}\text{CO}_2)$ in aliquots of whole air extracted from surveillance cylinders is 1.8%

139 (1 σ), roughly equating to 1 $\mu\text{mol mol}^{-1}$ C_{ff} detection capability from the measurement
140 uncertainty alone. The $\Delta(^{14}\text{CO}_2)$ data at AMY was tabulated in Table S1. Among four flasks, the
141 air from two flasks, after analysis for greenhouse gas mole fractions, was combined and analyzed
142 for $\Delta(^{14}\text{CO}_2)$.

143

144 **2.2 Data analysis method using $\Delta(^{14}\text{CO}_2)$ data**

145 **2.2.1 Calculation of C_{ff} and C_{bio}**

146 As Turnbull et al. (2009) suggested the observed CO_2 (C_{obs}) at AMY can be defined as:

147 $C_{\text{obs}} = C_{\text{bg}} + C_{\text{ff}} + C_{\text{other}} \quad (1)$

148 where C_{bg} , C_{ff} and C_{other} are the background, recently added fossil fuel CO_2 and the CO_2 derived
149 from the other sources.

150 According to Tans et al. (1993), the product of CO_2 abundance and its isotopic ratio is conserved;
151 the isotopic mass balance can be described as below:

152 $\Delta_{\text{obs}} C_{\text{obs}} = \Delta_{\text{bg}} C_{\text{bg}} + \Delta_{\text{ff}} C_{\text{ff}} + \Delta_{\text{other}} C_{\text{other}} \quad (2)$

153 where Δ is the $\Delta(^{14}\text{C})$ of each CO_2 component of Equ. (1).

154 Therefore we can calculate fossil fuel CO_2 by combining equations (1) and (2) as:

155 $C_{\text{ff}} = \frac{C_{\text{bg}}(\Delta_{\text{obs}} - \Delta_{\text{bg}})}{\Delta_{\text{ff}} - \Delta_{\text{bg}}} - \frac{C_{\text{other}}(\Delta_{\text{other}} - \Delta_{\text{bg}})}{\Delta_{\text{ff}} - \Delta_{\text{bg}}} \quad (3)$

156 Fossil fuel derived CO₂ contains no ¹⁴C because the half-life of ¹⁴C is (5700±30) years (Godwin,
157 1962) while these fuels are hundreds of millions of years old. As we mentioned in the section 1,
158 $\Delta(^{14}\text{CO}_2)$ is reported as a per mil (‰) deviation from the absolute radiocarbon reference standard
159 corrected for fractionation and decay with a simplified form; $\Delta(^{14}\text{C}) \approx [\text{R}_\text{sample}(^{14}\text{C}/\text{C}) / \text{R}_\text{standard}(^{14}\text{C}/\text{C}) - 1] 1000\text{‰}$, where $\text{R}_\text{sample}(^{14}\text{C}/\text{C})$ is the ¹⁴C/C amount ratio. Therefore Δ_{ff} is set at -
160 1000‰ (Stuiver and Pollach, 1977). Background values (Δ_{bg}) in equations (1) to (3) are
161 determined from measurements from background air collected at Niwot Ridge, Colorado, a high
162 altitude site at a similar latitude as AMY (NWR, 40.05° N, 105.58° W, 3,526 m a.s.l.). Turnbull
163 et al. (2011a) showed that the choice of background values did not significantly influence
164 derived enhancements due to the large regional and local signal at TAP, 28 km from AMY.
165 NWR $\Delta(^{14}\text{CO}_2)$ and other trace gas background values are selected using a flagging system to
166 exclude polluted samples (Turnbull et al., 2007), and then fitted with a smooth curve following
167 Thoning et al. (1989).

169 The second term of equation (3) is typically a small correction for the effect of other sources of
170 CO₂ that have a $\Delta(^{14}\text{C})$ differing by a small amount that of the atmospheric background, such as
171 CO₂ from the 1) nuclear power industry, 2) oceans, 3) photosynthesis and 4) heterotrophic
172 respiration.

173 1) The nuclear power industry produces ¹⁴C that can influence the C_{ff} calculation. South Korea
174 has nuclear power plants along the east coast that may influence AMY air samples when air-
175 masses originated from the eastern part of Korea (Figure 1). It is also possible that Chinese
176 nuclear plants could influence some samples. Here we did not make any correction for this since
177 most nuclear installations in this region are pressurized water reactors, which produce mainly ¹⁴C

178 in CH₄ rather than CO₂ (Graven and Gruber, 2011). 2) For the ocean, although there may also be
179 a small contribution from oceanic carbon exchange across the Yellow Sea, we consider this
180 effect small enough to ignore (Turnbull et al., 2011a). It was also demonstrated there is no
181 significant bias from the oceans including East China Sea (Song et al., 2018), even at coastal
182 sites in the Northern Hemisphere (Turnbull et al., 2009). Larger scale ocean exchange and also
183 stratospheric exchange affect both background and observed samples equally, so they can be
184 ignored in the calculations. 3) For the photosynthetic terms, ¹⁴C in CO₂ accounts for natural
185 fractionation during uptake, so we also set this observed value the same as the background value.
186 4) Therefore we only consider heterotrophic respiration. For land regions, where most fossil fuel
187 emissions occur, heterotrophic respiration could be a main contributor to the second term of
188 equation (3) due to ¹⁴C disequilibrium potentially. When this value is ignored, C_{ff} would be
189 consistently underestimated (Palstra et al., 2008; Riley et al., 2008; Hsueh et al., 2007; Turnbull
190 et al., 2006). For this, corrections were estimated as $(-0.2 \pm 0.1) \mu\text{mol mol}^{-1}$ during winter and $(-$
191 $0.5 \pm 0.2) \mu\text{mol mol}^{-1}$ during summer (Turnbull et al., 2009; Turnbull et al., 2006).

192 CO₂ enhancements relative to baseline CO₂ are defined as $\Delta x(\text{CO}_2)$, with the excess signal of
193 C_{obs} minus C_{bg} in Equ.(1). Partitioning of $\Delta x(\text{CO}_2)$ into C_{ff} and C_{bio} is calculated simply from the
194 residual of the difference between observed $\Delta x(\text{CO}_2)$ and C_{ff} .

195 2.2.2 The ratio of trace gas enhancement to C_{ff} and its correlation

196 To obtain the correlation coefficient (r) between C_{ff} and other trace gas enhancements ($\Delta x(x) =$
197 $x_{\text{obs}} - x_{\text{bg}}$) and the ratio of any trace gas to C_{ff} (R_{gas}), we use reduced major axis (RMA) regression
198 analysis (Sokal and Rohlf, 1981). The distributions of R_{gas} are normally broad and non-Gaussian

199 and RMA analysis is a relatively robust method of calculating the slope of two variables that
200 show some causative relationship. Here, x_{bg} was derived from NWR with the same method
201 described in section 2.2.1. The relevant equations are presented from Equ. S1 to Equ. S3. Results
202 for each species are given in Table 1.

203

204 **2.3 HYSPLIT cluster analysis**

205 HYSPLIT trajectories were run using Unified Model-Global Data Assimilation and Prediction
206 System (UM-GDAPS) weather data at 25 km by 25 km horizontal resolution to determine the
207 regions that influence air mass transport to AMY. A total of 70 air-parcel back-trajectories were
208 calculated for 72-h periods at 3-h intervals matching the time of each flask-air sample taken at
209 AMY from May 2014 to August 2016. We assign the sampling altitude as 500 m, since it was
210 demonstrated that HYSPLIT and other particle dispersion back-trajectory models (e.g.,
211 FLEXPART) are consistent at 500 m altitude (Li et al., 2014). Cluster analysis of the resulting
212 70 back-trajectories categorized six pathways through which air parcels arrive at AMY during
213 the time period of interest.

214 Among the calculated back-trajectories, 67% indicate air masses originating from the Asian
215 continent. Back-trajectories of continental background air (CB) originating in Russia and
216 Mongolia occurred 13% of the time. 23% of the trajectories originated and travelled through
217 northeast China (CN). The CN region includes Inner Mongolia and Liaoning, one of the most
218 populated regions in China with 43.9 million people in 2012. These CN air masses arrive in
219 South Korea after crossing through western North Korea. 17% of the trajectories are derived
220 from central eastern China around the Shandong area (CE). The CE region contains Shandianzi

221 (SDZ, 40.65° N, 117.12° E, 287 m a.s.l.) located next to the megacities of Beijing and Tianjin,
222 which are some of China's highest CO₂ emitting regions (Gregg et al., 2008). 14% are Ocean
223 Background (OB) derived from the East China Sea. Among them, a few of the trajectories
224 passed over the eastern part of China (e.g., over Shanghai) with high altitude (1000 m). Flow
225 from South Korea also travels through heavily industrialized and/or metropolitan regions in
226 South Korea (Korea Local, KL, 19%) and under stagnant conditions (Polluted Local region, PL,
227 14%). Some of the KL air-masses have also passed over the East Sea and Japan.

228

229 **3. Results and discussions**

230 **3.1 Observed $\Delta(^{14}\text{CO}_2)$ and portioning of CO₂ into C_{ff} and C_{bio}**

231 AMY $\Delta(^{14}\text{CO}_2)$ values are almost always lower than those observed at NWR, which we consider
232 to be broadly representative of background values for the mid-latitude Northern Hemisphere
233 (Figure 2). NWR $\Delta(^{14}\text{CO}_2)$, which is based on weekly air samples, was in the range 10.0 to 21.2
234 ‰, with an average $(16.6 \pm 3)\text{‰}$ (1σ , standard deviation) from May 2014 to August 2016.

235 Waliguan (WLG, 36.28° N, 100.9° E, 3816 m a.s.l.), an Asian background GAW station in
236 China, also showed similar $\Delta(^{14}\text{CO}_2)$ levels to NWR with an average of $(17.1 \pm 6.8)\text{‰}$ in 2015
237 (Niu et al., 2016, measurement uncertainty $\pm 3\text{‰}$, n=20). $\Delta(^{14}\text{CO}_2)$ at AMY varied from -59.5 to
238 23.1‰ and had a mean value of $(-6.2 \pm 18.8)\text{‰}$ (1σ , n=70) during the measurement period
239 (Table S1). This was similar to results from observations at SDZ, which is located about 100 km

240 northeast of Beijing, in the range of -53.0 to 32.6‰ with an average (-6.8 ± 21.1)‰ (1σ , $n=32$)

241 during Sep 2014 to Dec 2015 (Niu et al., 2016).

242 Calculated C_{ff} at AMY ranges between -0.05 and 32.7 $\mu\text{mol mol}^{-1}$ with an average of (9.7 ± 7.8)

243 $\mu\text{mol mol}^{-1}$ (1σ , $n=70$); high C_{ff} was observed regardless of season (Figure 2 (a)). One negative

244 C_{ff} value of -0.05 $\mu\text{mol mol}^{-1}$ was estimated due to greater AMY $\Delta(^{14}\text{CO}_2)$ than NWR on July 30,

245 2014. Although negative C_{ff} values are non-physical, this value is not significantly different from

246 zero, and is reasonable given that this air originated from the OB sector. The range of C_{ff} in the

247 AMY samples is similar to that observed at TAP from 2004 to 2010 (-1.6 to 42.9 $\mu\text{mol mol}^{-1}$

248 C_{ff}), but C_{ff} is on average about twice as high at AMY as in the 2004 to 2010 TAP samples

249 (mean (4.4 ± 5.7) $\mu\text{mol mol}^{-1}$, $n=202$) (Turnbull et al., 2011a). A more detailed comparison of

250 results based on differences between samples derived from the Asian continent and Korea local

251 air is provided in section 3.2.

252 Estimated C_{bio} , as defined in section 2.2.1, varied from -18.1 to 15.7 $\mu\text{mol mol}^{-1}$ (mean (0.9 ± 5.8)

253 $\mu\text{mol mol}^{-1}$) at AMY (Figure 2 (c)). C_{bio} showed a strong seasonal cycle with the lowest values

254 from July to September when photosynthetic drawdown is expected to be strongest, in good

255 agreement with the previous TAP study (Turnbull et al., 2011a). Even though C_{bio} was at times

256 negative, mainly due to photosynthesis during summer, the largest positive C_{bio} was also

257 observed in summer.

258 The largest C_{ff} by season was observed in order of winter (DJF, (11.3 ± 7.6), $n=14$) > summer

259 (JJA, (10.7 ± 9.2), $n=11$) > spring (MAM, (8.6 ± 8.0), $n=22$) > autumn (SON, (7.6 ± 5.6), $n=17$) with

260 a unit of $\mu\text{mol mol}^{-1}$. When we consider only positive contributions of C_{bio} samples, the order
261 was summer ((4.6 ± 4.0) , $n=14$) > autumn ((4.1 ± 2.5) , $n=9$) > spring ((3.8 ± 2.6) , $n=13$) > winter
262 ((3.4 ± 2.5) , $n=11$) with a unit of $\mu\text{mol mol}^{-1}$.

263 C_{ff} in summer was nearly as high as in winter. This is because lower wind speeds are observed at
264 AMY during summer (Lee et al., 2019). When we analyzed seasonal boundary layer height for
265 each sample by UM-GDAPS, it also showed similar result that it was highest in winter (with a
266 range from 150 m to 1100 m) and lowest in summer (with a range from 100 m to 500 m). This
267 suggests that these high summer C_{ff} values may reflect emission from local activities, which
268 were described in section 2.1, more than in other seasons.

269 The highest C_{bio} value was also observed in the summer, PL sector. PL sector showed that
270 positive C_{bio} correlates with CH_4 , which is a tracer for agriculture when observed in TAP local
271 air masses. Turnbull et al.(2011a) also showed similar results.

272 In winter, C_{bio} was relatively lower than in other seasons while C_{ff} was highest. During winter,
273 AMY is mainly affected by long-range transport of air-masses from China due to the Siberian
274 high (Lee et al., 2019). Therefore air samples were less affected by local activities in winter but
275 C_{bio} still contributed almost 23% to $\Delta x(\text{CO}_2)$. In the dry season (from October to March), forest
276 fires, which contribute the largest portion of total CO_2 emissions from open fires at the national
277 scale, are concentrated in northeastern and southern China (Yin et al., 2019). The highest CO_2
278 was observed in winter ((449.1 ± 244.1) nmol mol^{-1} (1σ) in winter while (236.8 ± 124.4) nmol
279 mol^{-1} (1σ) in summer), which also supports biomass burning and bio fuels as large contributors
280 to observed CO_2 enhancements in winter. Turnbull et al. (2011a) also showed that 20-30% of

281 winter CO₂ enhancements at TAP were likely contributed by biofuel combustion, along with
282 plant, soil, human, and animal respiration.

283 Regardless of the source, we find that C_{bio} contributes substantially to atmospheric CO₂
284 enhancements at AMY in air masses affected by local and long-range transport, so when only
285 CO₂ enhancements above background are compared to bottom-up inventories, it can make a bias
286 due to C_{bio} contributions.

287

288 3.2 C_{ff} comparison between Korea Local and Asian Continent samples

289 To more clearly identify samples originating from the Asian continent (trajectory clusters CB,
290 CN, CE, and OB) and Korea Local (trajectory cluster KL) after cluster analysis of the 70 sets of
291 measurements, we use wind speed data from the Automatic Weather System (AWS) installed at
292 the same level as the air sample inlet at AMY. Among the data from CB, CN, CE, OB, and KL,
293 when wind speed was less than 3 m/s, we assumed that those samples could be affected by local
294 pollution. PL was also ruled out since it was affected by local pollutions under the stagnant
295 condition. Therefore we use only 41 sets of observations for this analysis (Table 1).

296 C_{ff} is highest in the order CE > CN > KL > CB > OB (Table 1). During the measurement period,
297 the averages from Asian continent (sectors CE and CN) were higher than KL without the
298 baseline sector (CB and OB). The calculated mean C_{ff} using only CE, CN, CB and OB, which
299 sample substantial outflow from the Asian Continent, was $(7.6 \pm 3.9) \mu\text{mol mol}^{-1}$.

300 When we compared the KL samples ($(8.6 \pm 5.3) \mu\text{mol mol}^{-1}$) with those from Korea Local air-
301 masses observed at TAP ($(8.5 \pm 8.6) \mu\text{mol mol}^{-1}$, $n=58$, Turnbull et al., 2011a), mean C_{ff} was
302 quite similar (Figure 3). However, when comparing the C_{ff} values from CB air masses in this
303 study and TAP far-field (from China) samples ($n=144$, Turnbull et al., 2011a), C_{ff} almost
304 doubled from $(2.6 \pm 2.4) \mu\text{mol mol}^{-1}$ to $(4.3 \pm 2.1) \mu\text{mol mol}^{-1}$, even though they might be expected to have
305 had similar air mass back-trajectories. We also compared the values at SDZ from 2009 to 2010
306 (Turnbull et al., 2011a) and in 2015 (Niu et al., 2016); they also increased, not only in the
307 samples that were affected by Beijing and North China Plain (SDZ-BN), which are comparably
308 polluted, but also in the samples that were affected by northeast China (SDZ-NE). For SDZ-BN
309 samples, C_{ff} increased from $(10 \pm 1) \mu\text{mol mol}^{-1}$ from 2009/2010 ($n=32$) to 2015
310 ($n=32$). The AMY samples from CE, which flow over Beijing, showed $(11.2 \pm 8.3) \mu\text{mol mol}^{-1}$ of
311 C_{ff} and were also slightly greater than the 2009 – 2010 SDZ-BN samples (Turnbull et al., 2011a).
312 For SDZ-NE samples, C_{ff} was $(3 \pm 7) \mu\text{mol mol}^{-1}$ in 2009 to 2010 and increased to $(7.6 \pm 6.8) \mu\text{mol mol}^{-1}$ in 2015. Since the SDZ-NE samples are affected by northeast China according to
313 Turnbull et al. (2011a) and Niu et al. (2016), we also see CN that originated from northeast china
314 (NE) and its mean value of C_{ff} had increased around $(10.6 \pm 6.9) \mu\text{mol mol}^{-1}$ compared to those
315 values in 2009 to 2010.
316 It has been suggested that inter-annual variability in observed mean C_{ff} in South Korea could
317 reflect changing fossil fuel CO_2 emissions, or could indicate inter-annual variability in the air
318 mass trajectories of the (small) dataset of flask-air samples (Turnbull et al., 2011a). Even though
319

320 the growth rate of C_{ff} emission has been decreasing slowly in East Asia since 2010 due to
321 emission reduction policies (Labzovskii et al., 2019), reported emissions increased 16.7% in
322 China and 1.8% in South Korea from 2010 to 2016 (Janssens-Maenhout et al., 2017). This is
323 broadly consistent with the flat trend in observed C_{ff} in KL air masses, and in the upward trend in
324 C_{ff} observed in air-masses flowing out from Asia. Therefore it is possible that AMY mean C_{ff}
325 increased relative to the earlier TAP observations due to increased fossil fuel emissions from the
326 Asian continent.

327 On the other hand, those values from this study showed large variability with small sample
328 numbers due to different sampling strategy, environment, and synoptic conditions such as
329 boundary layer height at the sampling time from reference studies. Further study will be
330 necessary to understand those increased values.

331

332 **3.3. Correlation of C_{ff} with SF_6 and its emission ratios**

333 We calculated correlation coefficients (r from Equ. (S3)) between SF_6 and CO enhancements
334 with C_{ff} and their ratios from Equ. (S1) with the 50 samples that were described in section 3.2
335 including PL sector ($n=9$) and whose values are tabulated in Table 1.

336 The correlations of CO enhancements ($\Delta x(CO)$) with C_{ff} were strong ($r > 0.7$) in all sectors
337 except PL, while SF_6 enhancements ($\Delta x(SF_6)$) correlated strongly with C_{ff} ($r > 0.8$) for CE and
338 OB in outflow from the Asian Continent and KL. R_{CO} and R_{SF_6} were different between Korea
339 Local and outflows from the Asian Continent. Here we discuss R_{SF_6} and section 3.4 discuss R_{CO}
340 more detail.

341 For SF₆, observed mean levels were high in order of (KL, PL) > (CN, CE) > (OB, CB) (Table 1).
342 SF₆ in KL and PL were higher than from the Asian Continent, since South Korea has larger SF₆
343 emissions than most countries (ranked at 4th as of 2010 according to the EDGAR4.2.) because of
344 liquid-crystal display (LCD) and electrical equipment production (Fang et al., 2014). Even
345 though both KL and PL showed higher SF₆ mole fraction than outflows of Asian Continent, the
346 correlation is different between KL and PL (Table 1). Under stagnant conditions, emitted SF₆ is
347 less diluted by mixing, so that in PL, $\Delta x(SF_6)$ correlated weakly with C_{ff} . On the other hand, KL,
348 CE and OB showed strong correlations ($r > 0.8$). Those three sectors are also larger SF₆ sources
349 compared to other regions, according to SF₆ emission estimates for Asia (Fang et al., 2014).
350 Because long-range transport allows time for mixing, SF₆ and C_{ff} emissions are effectively co-
351 located at not only continental scales but also regional scales. Thus SF₆ can be a good tracer of
352 fossil fuel CO₂ for those regions.

353 The correlation between $\Delta x(SF_6)$ and C_{ff} was strong in CE, OB and KL, however, R_{SF6} is
354 different between South Korea and outflow from the Asian continent (Figure S2). In a previous
355 study, observed R_{SF6} was 0.02 to 0.03 pmol μmol^{-1} at NWR in 2004 (Turnbull et al., 2006). Here,
356 the ratio was at (0.19 ± 0.03) and (0.17 ± 0.03) pmol μmol^{-1} for CE and OB respectively. For KL,
357 it was (0.66 ± 0.16) pmol μmol^{-1} indicating much larger ratios than in outflow from the Asian
358 continent. Further, observed R_{SF6} is 2 to 3 times greater for all air masses than predicted from
359 bottom-up inventories based on national scale roughly. For this calculation, we use EDGAR4.3.2
360 for CO₂ and EDGAR4.2 for SF₆. We repeat the calculations for both CO₂ and SF₆ with Korea's
361 National Inventory Report (KNIR, Greenhouse Gas Inventory and Research Center, 2018).
362 Using SF₆ for 2010 from EDGAR4.2, we obtain R_{SF6} of 0.08 pmol μmol^{-1} for China while for

363 South Korea it was $0.14 \text{ pmol } \mu\text{mol}^{-1}$. Especially for South Korea, this is much lower than the
364 observed R_{SF_6} . When KL R_{SF_6} was compared to ratios calculated from the KNIR inventory (0.27
365 $\text{pmol } \mu\text{mol}^{-1}$ for 2010 and $0.22 \text{ pmol } \mu\text{mol}^{-1}$ for 2014), it was closer to observed R_{SF_6} than
366 EDGAR, but still underestimated (Figure S3 and S2). This result suggests that the observed ratio
367 could be used to re-evaluate the bottom-up inventories (Rivier et al., 2006), especially targeting
368 the Asian continent. Even though KL R_{SF_6} showed greater uncertainty than CE and OB, it is still
369 greater than bottom-up inventories, such as KNIR and EDGAR. Therefore it would be useful to
370 get more data to try and derive a more robust estimate to evaluate SF_6 emission inventories for
371 Korea.

372

373 **3.4 Correlation of C_{ff} with CO and its emission ratios**

374 High CO was mainly observed in outflow from the Asian continent in order of $\text{CE} > \text{CN} > \text{PL} >$
375 $(\text{CB}, \text{KL}) > \text{OB}$ (Table 1). The order of CO is quite different to that of SF_6 . CO from KL and PL
376 is lower than from outflow from the Asian continent, except for the OB sector, indicating that
377 high CO can be a tracer of outflow from the Asian continent. Since CO is produced during
378 incomplete combustion of fossil fuel and biomass, it is more closely related to fossil fuel CO_2
379 emissions than the other trace gases. Therefore in most cases the correlation between CO and C_{ff}
380 was strong. R_{CO} was very different between air masses originating from South Korea Local
381 $((8 \pm 2) \text{ nmol } \mu\text{mol}^{-1})$ and the Asian continent $((29 \pm 8) \text{ to } (36 \pm 2) \text{ nmol } \mu\text{mol}^{-1})$, due to differences
382 in combustion efficiencies and the use of catalytic converters. The higher continental emission
383 ratios may also result from some contribution of biofuel combustion and agricultural burning in
384 the Asian continent, which have significantly higher CO emission than fossil-fuel combustion

385 (Akagi et al., 2011). For example, for CB the CO level is similar to KL while R_{CO} is higher than
386 KL with low C_{ff} .

387 Typically CO shows seasonal variations with lower values in summer due to the atmospheric
388 chemical sink, OH. Among the samples, the samples collected in summer were mainly rejected
389 through wind speed cut-off (less than 3 m/s) since AMY has lower wind speed in summer (Lee
390 et al., 2019). Only OB sector includes 4 summer samples (of 7), because summer air masses are
391 mainly from the southern part of the Yellow Sea (Lee et al., 2019). However, we assumed R_{CO} is
392 less affected by the summer sink, since only two $\Delta x(CO)$ samples were negative for OB (Figure
393 S1) and R_{CO} was consistent whether or not the negative $\Delta x(CO)$ values were considered. To
394 compare emission ratios derived from atmospheric observations with those from inventories for
395 2000 to 2012, we calculated inventory emission ratio (I_{CO/CO_2}) as:

396
$$I_{CO/CO_2} = E_{CO}/E_{CO_2} \times M_{CO_2}/M_{CO}$$

397 Where, E_{CO} and E_{CO_2} are total CO and fossil fuel CO_2 emissions in gigagrams ($Gg\ a^{-1}$, $10^9\ g\ a^{-1}$)
398 from the bottom-up national inventory. M_X is the molar masses of CO and CO_2 in $g\ mol^{-1}$.

399 We use EDGAR4.3.2 (Janssens-Maenhout et al., 2017) and KNIR (Greenhouse Gas Inventory
400 and Research Center, 2018) for inventory information for both CO and CO_2 .

401 The uncertainty of EDGAR4.3.2 fossil fuel CO_2 emissions was reported as a 95% confidence
402 interval (Janssens-Maenhout et al., 2019), $\pm 5.4\%$ for China and $\pm 3.6\%$ for South Korea
403 (personal communication with Dr. Efisio Solazzo). The uncertainties of CO and SF_6 emissions
404 were not reported by EDGAR. For KNIR, the CO_2 2016 emission uncertainty in the energy

405 sector was $\pm 3\%$ (Greenhouse Gas Inventory and Research Center, 2018). KNIR does not provide
406 uncertainties for other emission sectors of CO_2 , nor from emissions of CO and SF_6 .

407 In Fig. 4 we confirm that the CO to C_{ff} emission ratios (R_{CO}) derived from both observations and
408 inventories for China and South Korea are decreasing. Since C_{ff} emissions appear to be flat
409 (South Korea) or slightly increasing (China), this indicates that combustion efficiency and/or
410 scrubbing of CO is improving.

411 For South Korea, EDGAR4.3.2 indicated that CO emissions from the energy sector (98% to 99%
412 of total emission) decreased by 47% between the 1997 and 2012. South Korean fossil fuel CO_2
413 emissions increased until 2011 and remained mostly constant from 2011 to 2016
414 ($(603,901 \pm 4,315) \text{ Gg a}^{-1} \text{ CO}_2$) (Figure S4). Therefore the decreased trend in the emission ratio
415 seems to reflect recent decreases in CO emissions in South Korea. Turnbull et al. (2011a)
416 determined an observed mean R_{CO} of $(13 \pm 3) \text{ nmol } \mu\text{mol}^{-1}$ during 2004 to 2010. Suntharalingam
417 et al. (2004) estimated R_{CO} $15.4 \text{ nmol } \mu\text{mol}^{-1}$ for South Korea in 2001 from CO_2 and CO airborne
418 observations (C_{ff} was not determined). Recently, the KORUS-AQ campaign, which was
419 conducted over Seoul from May to June in 2016, estimated R_{CO} as $9 \text{ nmol } \mu\text{mol}^{-1}$ (Tang et al.,
420 2018) based on CO_2 and CO observations (C_{ff} was not determined). Our study gives R_{CO} of (8 ± 2)
421 $\text{nmol } \mu\text{mol}^{-1}$ for South Korea, slightly but not significantly lower than the KORUS-AQ result for
422 Seoul. Different contributions of C_{bio} and C_{ff} to total CO_2 may bias the R_{CO} calculation when
423 total CO_2 was used in the KORUS-AQ study (e.g., Miller et al., 2012). The South Korean
424 national R_{CO} from EDGAR4.3.2 in 2012 was $6.7 \text{ nmol } \mu\text{mol}^{-1}$, consistent with our observations.
425 Using KNIR for 2016, we obtain R_{CO} of $2.1 \text{ nmol } \mu\text{mol}^{-1}$. KNIR suffers from a large number of

426 missing CO emission sources compared to the EDGAR, as indicated by their reported emissions,
427 638.3 and 2580.8 Gg a^{-1} in 2012, respectively (Figure S5). For example, CO emissions recently
428 derived from fugitive emissions and residential/other sectors increased to 14% and 11.5% of total
429 emission respectively in EDGAR but were not reported in KNIR.

430 For China the inventories estimate that CO emissions from the energy sector, $(96.5 \pm 0.2)\%$, were
431 almost constant through the 1990s, and then increased during the early-2000s from industrial
432 processes (8.8% of total emissions in 2012). Fossil fuel CO₂ emission in China also increased
433 until 2013 and then stayed roughly constant at $(10,461,890 \pm 60,571)$ Gg a^{-1} according to
434 EDGAR4.3.2. Thus even though both emissions show an increase from 2000 to 2016 for fossil
435 fuel CO₂ and to 2012 for CO, the emission ratio decreased (Figure S4 and Figure 4) seeming to
436 indicate that combustion efficiency is improving. Many studies observed decreasing R_{CO} in
437 China from 2000 to 2010 (Turnbull et al., 2011a; Wang et al., 2010). Suntharalingam et al. (2004)
438 reported R_{CO} was 55 nmol μmol^{-1} in 2001 (C_{ff} was not determined). In the Beijing region, R_{CO}
439 decreased from 57.80 to 37.59 nmol μmol^{-1} during 2004 to 2008 (Wang et al., 2010). The overall
440 R_{CO} was (47 ± 2) nmol μmol^{-1} at SDZ for 2009-2010 and (44 ± 3) nmol μmol^{-1} in air-masses that
441 originated from the Asian continent from 2005 to 2009 (Turnbull et al., 2011a). Tohjima et al.
442 (2014) explained that surface based R_{CO} decreased from 45 to 30 nmol μmol^{-1} in outflow air
443 masses from China from 1998 to 2010. Fu et al. (2015) also observed R_{CO} of 29 nmol μmol^{-1}
444 over mainland China in 2009. In Beijing, which is located along the path of CE, it was (30.4 ± 1.6)
445 nmol μmol^{-1} and (29.6 ± 3.2) nmol μmol^{-1} for Xiamen in 2016, which is in the OB sector (Niu et
446 al., 2018). During KORUS-AQ in 2016, R_{CO} of 28 nmol μmol^{-1} was observed over the Yellow

447 Sea. Some of those studies did not differentiate C_{ff} from the total CO₂ enhancement, so, although
448 R_{CO} still includes uncertainties, it is continually decreasing.

449 In this study R_{CO} is (29±8), (31±8), (36±2), and (31±4) nmol μmol^{-1} for CB, CN, CE and OB,
450 consistent with Tang et al.(2018) and Liu et al.(2018). On the other hand, R_{CO} in CE is higher
451 than in other sectors in this study. The Shandong area, which is located in the path of CE, has
452 been plagued with problems of combustion inefficiency and ranked as the largest consumer of
453 fossil fuels in all of China (Chen and Li, 2009). The uncertainties in our observed R_{CO} for this
454 region overlap with other sectors such as CB, CN and OB, so further monitoring of the ratios
455 will help to get more detailed information.

456 In South Korea and China, atmosphere-based R_{CO} values calculated by this study are (1.2±0.3)
457 times (with KL), (1.6±0.4), (1.7±0.4), (2±0.1) and (1.7±0.2) times greater (with CB, CN, CE
458 and OB) than in the inventory, respectively (Figure 4). This is in agreement with previous studies
459 (Turnbull et al., 2011a; Kurokawa et al., 2013; Tohjima et al., 2014). One explanation is that
460 EDGAR does not reflect secondary CO production, which can be a significant contributor to CO
461 (Kurokawa et al., 2013). Also, CO derived from biomass burning and biofuels was not included
462 in this inventory. Therefore, this indicates that top-down observations are necessary to evaluate
463 and improve bottom-up emission products.

464

465 **4. Summary and Conclusions**

466 To understand CO₂ sources and sinks in Korea as well as those of the surrounded region, we
467 collected $\Delta(^{14}\text{CO}_2)$ with 70 flask samples from May 2014 to August 2016. We summarized our
468 results below.

469 1) Observed $\Delta(^{14}\text{CO}_2)$ values at AMY ranged from -59.5 to 23.1‰ (a mean value of
470 (-6.2±18.8)‰ (1σ)) during the study period, almost always lower than those observed at
471 NWR, which we consider to be broadly representative of background values for the mid-
472 latitude Northern Hemisphere. This reflects the strong imprint of fossil fuel-CO₂
473 emissions recorded in AMY air samples.

474 2) Calculated C_{ff} using $\Delta(^{14}\text{CO}_2)$ at AMY ranges between -0.05 and 32.7 $\mu\text{mol mol}^{-1}$ with
475 an average of (9.7±7.8) $\mu\text{mol mol}^{-1}$ (1σ); this average is twice as high as in the 2004 to
476 2010 TAP samples (mean (4.4±5.7) $\mu\text{mol mol}^{-1}$) (Turnbull et al., 2011a). We also
477 observed high C_{ff} regardless of the season or source region. After separately identifying
478 samples originating from the Asian continent and the Korean peninsula, we determined
479 that the mean C_{ff} increased relative to the earlier observations due to increased fossil fuel
480 emissions from the Asian continent as showing by the consistent growth in reported
481 emissions, which increased 16.7% in China and only 1.8% in South Korea from 2010 to
482 2016. Note, however, that our data span a relatively limited time period and are subject
483 to different synoptic conditions during the sampling time from previous studies, so a
484 longer time-series would increase confidence in tracking this change.

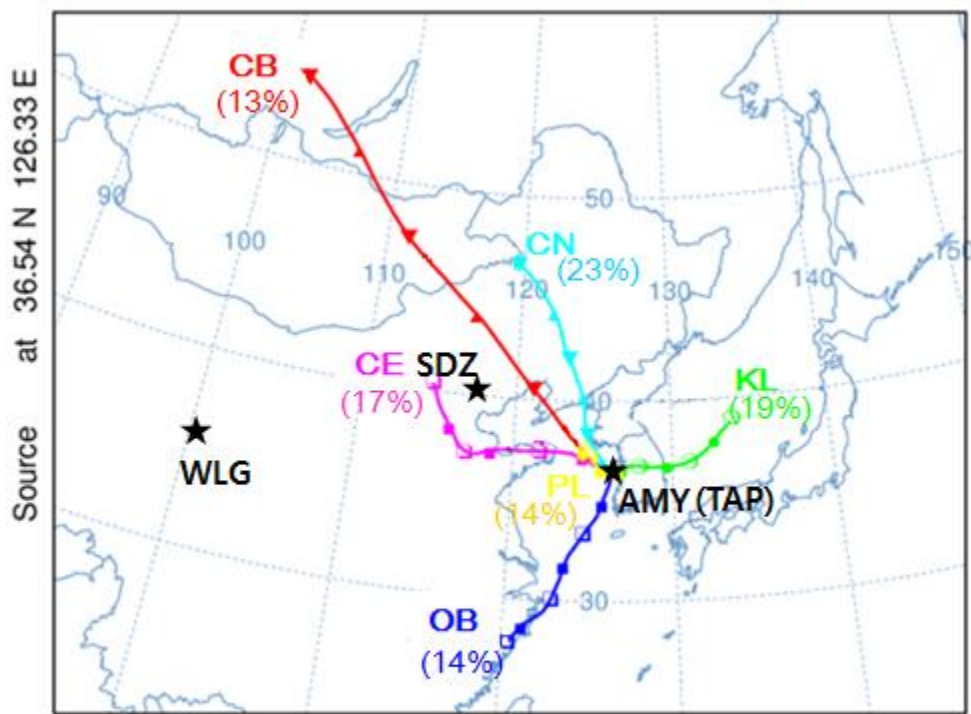
485 3) Because $\Delta x(\text{CO})$ and $\Delta x(\text{SF}_6)$ agreed well with C_{ff} , but showed different slopes for Korea
486 and the Asian continent, those R_{gas} values can be indicators of air mass origin and those

487 gases can be proxies for C_{ff} . Overall, we have confirmed that both R_{CO} derived from
488 inventory and observation have decreased relative to previous studies, indicating that
489 combustion efficiency is increasing in both China and South Korea.

490 4) However, atmosphere-based R_{gas} values are greater than bottom-up inventories. For CO,
491 our values are (1.2 ± 0.3) times and (1.6 ± 0.4) to (2.0 ± 0.1) times greater than in inventory
492 values for South Korea and China, respectively. This discrepancy may arise from several
493 sources including the no contribution of atmospheric chemical CO production such as
494 oxidation of CH_4 and non-methane VOCs. Observed R_{SF6} is 2 to 3 times greater than in
495 inventories. Therefore those values in our study can be used for improving bottom-up
496 inventories in the future.

497 5) Finally, we stress that because C_{bio} contributes substantially to $\Delta x(CO_2)$, even in winter,
498 $\Delta^{14}C$ -based C_{ff} (and not $\Delta x(CO_2)$) is required for accurate calculation of both R_{CO} and
499 R_{SF6} .

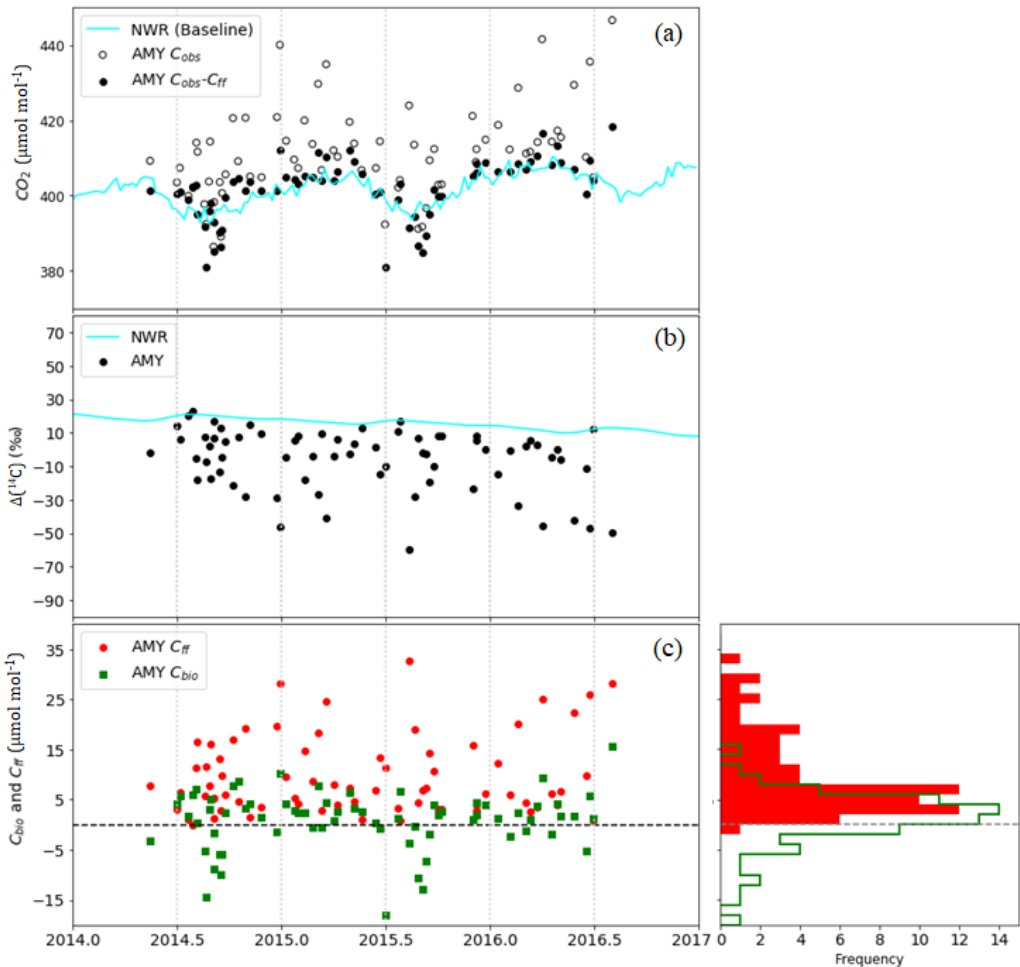
500



501

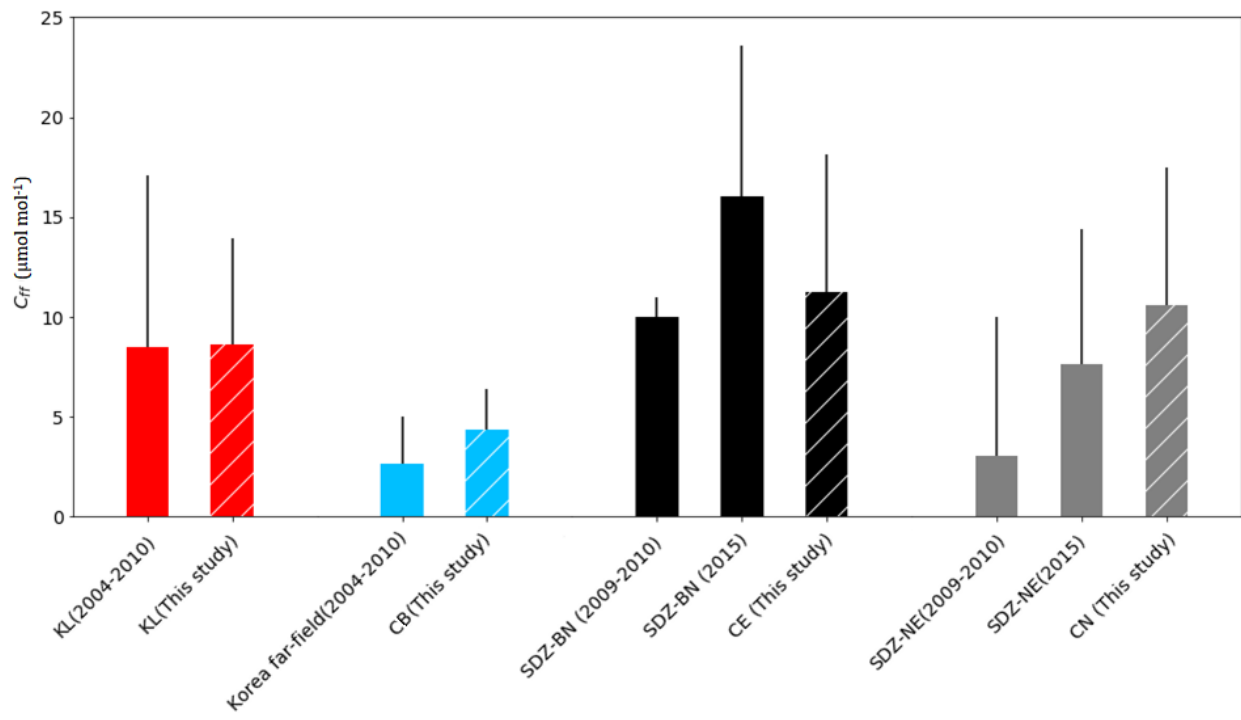
502 Figure 1. A total of 70 air-parcel back-trajectories were calculated for 72-h periods at 3-h
 503 intervals from May 2014 to August 2016 using the HYSPLIT model in conjunction with KMA
 504 UM GDAPS data at 25 km by 25 km resolution. Station locations are: WLG (Waliguan, 36.28°
 505 N, 100.9° E, 3816 m a.s.l.), SDZ (Shandianzi, 40.65° N, 117.12° E, 287 m a.s.l.), and AMY
 506 (Anmyeondo, 36.53° N, 126.32° E, 86 m a.s.l.). TAP (Tae-Ahn Peninsula, 36.73° N, 126.13° E,
 507 20 m a.s.l.) is around 28 km northeast from AMY.

508

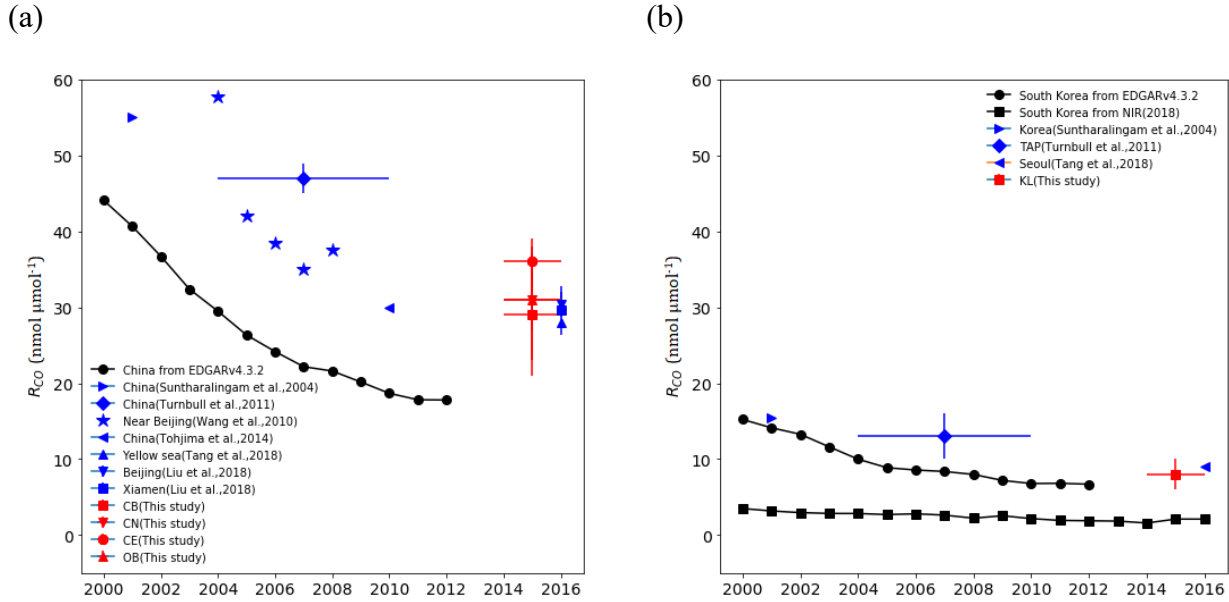


509
510 Figure 2. Time series of (a) observed CO₂ dry air mole fraction (open circles) and observed CO₂
511 (C_{obs}) minus C_{ff} calculated from Δ(¹⁴CO₂) (closed circles). (b) Δ(¹⁴CO₂) at AMY (black circles)
512 and at NWR (Niwot Ridge, line), baseline data. (c) Time series of C_{ff} and C_{bio} calculated from
513 Δ(¹⁴CO₂) (left) and the frequency distribution at AMY (right).

514



517 Figure 3. Calculated C_{ff} ($\mu\text{mol mol}^{-1}$). Red bars are for KL and blue bars are for Korea far-field
 518 (China) (2004-2010 from Turnbull et al. (2011a)). Black bars are for SDZ-BN samples that were
 519 affected by Beijing and North China plain. Gray bars for SDZ-NE indicate samples that were
 520 affected by regions northeast of SDZ. SDZ (2009-2010) is from Turnbull et al. (2011a) and SDZ
 521 (2015) is from Niu et al. (2016). Hatched red, blue, black and grey bars are derived from this
 522 study during 2014 to 2016.



523 Figure 4. R_{CO} for China (a) and for South Korea (b). Black circles: EDGARv4.3.2 emission
 524 inventory. Black squares: National Inventory Report, Korea (2018). Blue symbols are from other
 525 studies (Suntharalingam et al., 2004; Wang et al., 2010; Turnbull et al., 2011a; Tohjima et al.,
 526 2014; Liu et al., 2018; Tang et al., 2018). Red symbols: This study. Y-error bars: uncertainty in
 527 the slope according to equation (S2). X-error bars: the period for the mean value.

528

529 Table 1. Means and standard deviations of C_{ff} ($\mu\text{mol mol}^{-1}$), CO (nmol mol^{-1}) and SF_6 (pmol mol^{-1}) (total N=50, without PL N=41). The correlations (r) and the ratio (R_{gas}) of enhancement
 530 between C_{ff} were determined by Reduced Major Axis (RMA) regression analysis on each scatter
 531 plot to obtain regression slopes. The uncertainty of R_{gas} refers to equation (S2). When r is less
 532 than 0.7, R_{gas} was not included here. N is the number of data. The unit of R_{CO} is $\text{nmol } \mu\text{mol}^{-1}$ and
 534 for R_{SF_6} it is $\text{pmol } \mu\text{mol}^{-1}$. A plot of R_{CO} and R_{SF_6} is shown in Figure S1. CB represents
 535 continental background, CN north east China, CE central eastern China, OB ocean background,
 536 KL Korea local and PL polluted local air-mass

	Outflow from the Asia continent				South Korea	
	CB (N=7)	CN (N=9)	CE (N=9)	OB (N=7)	KL (N=9)	PL (N=9)
C_{ff}	4.3 \pm 2.1	10.6 \pm 6.9	11.2 \pm 8.3	4.1 \pm 2.7	8.6 \pm 5.3	15.6 \pm 11.6
CO	233 \pm 59	353 \pm 219	473 \pm 293	169 \pm 90	228 \pm 40	259 \pm 100
SF_6	9.0 \pm 0.4	10.1 \pm 1.2	10.1 \pm 1.5	9.2 \pm 0.5	13.0 \pm 3.3	12.7 \pm 6.2
R_{CO} (r)	29 \pm 8 (0.80)	31 \pm 8 (0.76)	36 \pm 2 (0.98)	31 \pm 4 (0.96)	8 \pm 2 (0.74)	- (0.44)
R_{SF_6} (r)	- (0.63)	- (0.48)	0.19 \pm 0.03 (0.91)	0.17 \pm 0.03 (0.94)	0.66 \pm 0.16 (0.76)	- (0.38)

537
 538

539 **Data availability**
540
541 Our CO₂, CO, SF₆ data from AMY and NWR can be downloaded from
542 ftp://aftp.cmdl.noaa.gov/data/trace_gases. $\Delta(^{14}\text{CO}_2)$ data are provided in the supplementary
543 material of this paper.

544

545 **Author contributions**
546 HL wrote this paper and analyzed all data. HL and GWL designed this study. EJD and JCT
547 guided and reviewed this paper. SL collected samples and gave the information of the data at
548 AMY. EJD, JCT, SJL, JBM, GP, and JL provided data and reviewed the manuscript. All authors
549 contributed this work.

550

551 **ACKNOWLEDGMENT**

552 This work was funded by the Korea Meteorological Administration Research and Development
553 Program "Research and Development for KMA Weather, Climate, and Earth system Services—
554 Development of Monitoring and Analysis Techniques for Atmospheric Composition in Korea"
555 under Grant (KMA2018-00522).

556

557 **REFERENCES**

558 Akagi, S. K., R. J. Yokelson, C. Wiedinmyer, M. J. Alvarado, J. S. Reid, T. Karl, J. D. Crouse,
559 P. O. Wennberg: Emission factors for open and domestic biomass burning for use in atmospheric
560 models, *Atmos. Chem. Phys.* 11, 4039-4027, doi:10.5194/acp-11-4039-2011, **2011**

561 Boden, T.A., G. Marland, and R.J. Andres: National CO₂ Emissions from Fossil-Fuel Burning,
562 Cement Manufacture, and Gas Flaring: 1751-2014, Carbon Dioxide Information Analysis Center,
563 Oak Ridge National Laboratory, U.S. Department of Energy, doi 10.3334/CDIAC/00001_V2017,
564 **2017**

565 Chen, Y. Y. Li: Low-carbon economy and China's regional energy use research. *Jilin Univ. J.*
566 *Soc. Sci. Ed.* 49(2), 66-73, **2009**

567 Fang, X., R. L. Thompson, T. Saito, Y. Yokouchi, J. Kim, S. Li, K. R. Kim, S. Park, F. Graziosi,
568 A. Stohl: Sulfur hexafluoride (SF₆) emissions in East Asia determined by inverse modeling.
569 *Atmos. Chem. Phys.* 14, 4779–4791, doi:10.5194/acp-14-4779-2014, **2014**

570 Fu, X. W., H. Zhang, C.-J. Lin, X. B. Feng, L. X. Zhou, S. X. Fang: Correlation slopes of
571 GEM/CO, GEM/CO₂, and GEM/CH₄ and estimated mercury emissions in China, South Asia, the
572 Indochinese Peninsula, and Central Asia derived from observations in northwestern and
573 southwestern China. *Atmos. Chem. Phys.* 15, 1013-1028, doi:10.5194/acp-15-1013-2015, **2015**

574 Gamnitzer, U., U. Karstens, B. Kromer, R. E. M. Neubert, H. Schroeder, I. Levin: Carbon
575 monoxide: A quantitative tracer for fossil fuel CO₂?. *J. Geophys. Res.*, 111, D22302,
576 doi:10.1029/2005JD006966, **2006**

577 Geller, L. S., J. W. Elkins, J. M. Lobert, A. D. Clarke, D. F. Hurst, J. H. Butler, R. C. Myers:
578 Tropospheric SF₆: Observed latitudinal distribution and trends, derived emissions and
579 interhemispheric exchange time. *Geophys. Res. Lett.*, 24(6), 675–678, doi:10.1029/97GL00523,
580 **1997**

581 Graven, H. D. N. Gruber: Continental-scale enrichment of atmospheric $^{14}\text{CO}_2$ from the nuclear
582 power industry: Potential impact on the estimation of fossil fuel-derived CO_2 . *Atmos. Chem.*
583 *Phys. Discuss.* **11**, 14,583–14,605, doi:10.5194/acpd-11-14583-2011, **2011**

584 Graven, H. D., B. B. Stephens, T. P. Guilderson, T. L. Campos, D. S. Schimel, J. E. Campbell, R.
585 F. Keeling: Vertical profiles of biospheric and fossil fuel-derived CO_2 and fossil fuel $\text{CO}_2:\text{CO}$
586 ratios from airborne measurements of ^{14}C , CO_2 and CO above Colorado, USA, *Tellus*, **61**, 536–
587 546, DOI:10.1111/j.1600-0889.2009.00421.x, **2009**

588 Gregg, J. S. R. J. Andres, G. Marland: China: Emissions pattern of the world leader in CO_2
589 emissions from fossil fuel consumption and cement production, *Geophys. Res. Lett.* **35**, L08806,
590 doi:10.1029/2007GL032887, **2008**

591 Greenhouse Gas Inventory and Research Center: National Greenhouse Gas Inventory Report of
592 Korea; National statistics-115018, 11-1480906-000002-10,
593 www.gir.go.kr/home/index.do?menuId=36 (in Korean), **2018**

594 Hsueh, D. Y., N. Y. Krakauer, J. T. Randerson, X. Xu, S. E. Trumbore, J. R. Sounth: Regional
595 patterns of radiocarbon and fossil fuel derived CO_2 in surface air across North America, *Geophys.*
596 *Res. Lett.*, **34**, L02816, doi:10.1029/2006GL027032, **2007**

597 Janssens-Maenhout, G., M. Crippa, D. Guizzardi, M. Muntean, E. Schaaf, J.G.J. Olivier,
598 J.A.H.W. Peters, K.M. Schure: Fossil CO_2 and GHG emissions of all world countries, EUR
599 28766 EN, Publications Office of the European Union, Luxembourg, ISBN 978-92-79-73207-2,
600 doi:10.2760/709792, JRC107877, **2017**

601 Janssens-Maenhout, G.; M. Crippa, D. Guizzardi, M. Muntean, E. Schaaf, F. Dentener, P.
602 Bergamaschi, V. Pagliari, J. G. J. Olivier, J. A. H. W. Peters, J. A. van Aardenne, S. Monni, U.
603 Doering, A. M. R. Petrescu, E. Solazzo, G. D. Oreggioni: EDGAR v4.3.2 Global Atlas of the
604 three major greenhouse gas emissions for the period 1970–2012, *Earth Syst. Sci. Data*, **11**, 959–
605 1002, <https://doi.org/10.5194/essd-11-959-2019>, **2019**

606 Kurokawa, J., T. Ohara, T. Morikawa, S. Hanayama, G. Janssens-Maenhout, T. Fukui, K.
607 Kawashima, H. Akimoto: Emissions of air pollutants and greenhouse gases over Asian
608 regions during 2000–2008: Regional Emission inventory in ASia (REAS) version 2, *Atmos.*
609 *Chem. Phys.* **13**, 11019–11058, doi:10.5194/acp-13-11019-2013, **2013**

610 Labzovskii, L.D., H. W. L. Mak, S. T. Kenea, J.-S. Rhee, A. Lashkari, S. Li, T.-Y. Goo, Y.-S.
611 Oh, Y.-H. Byun: What can we learn about effectiveness of carbon reduction policies from
612 interannual variability of fossil fuel CO₂ emissions in East Asia? *Environ. Sci. Policy.* **96**, 132–
613 140, <https://doi.org/10.1016/j.envsci.2019.03.011>, **2019**

614 Lee, H., S.-O. Han, S.-B. Ryoo, J.-S. Lee, G.-W. Lee: The measurement of atmospheric CO₂ at
615 KMA GAW regional stations, its characteristics, and comparisons with other East Asian sites.
616 *Atmos. Chem. Phys.* **19**, 2149–2163, doi.org/10.5194/acp-19-2149-2019, **2019**

617 Lehman, S.J., J. B. Miller, C. Wolak, J.R. Sounthor, P.P. Tans, S.A. Montzka, C. Sweeney, A. E.
618 Andrews, B.W. LaFranchi, T. P. Guilderson: Allocation of terrestrial carbon sources using ¹⁴CO₂:
619 methods, measurement, and modelling. *Radiocarbon*. **55**(2–3):1484–95, **2013**

620 Le Quéré, C., R. M. Andrew, P. Friedlingstein, S. Sitch, J. Hauck, J. Pongratz, P. A. Pickers, J. I.
621 Korsbakken, G. P. Peters, J. G. Canadell, A. Arneth, V. K. Arora, L. Barbero, A. Bastos, L. Bopp,

622 F. Chevallier, L. P. Chini, P. Ciais, S. C. Doney, T. Gkrizalis, D. S. Goll, I. Harris, V. Haverd, F.
623 M. Hoffman, M. Hoppema, R. A. Houghton, G. Hurt, T. Ilyina, A. K. Jain, T. Johannessen, C. D.
624 Jones, E. Kato, R. F. Keeling, K. K. Goldewijk, P. Landschützer, N. Lefèvre, S. Lienert, Z. Liu,
625 D. Lombardozzi, N. Metzl, D. R. Munro, J. E. M. S. Nabel, S. Nakaoka, C. Neill, A. Olsen, T.
626 Ono, P. Patra, A. Peregon, W. Peters, P. Peylin, B. Pfeil, D. Pierrot, B. Poulter, G. Rehder, L.
627 Robertson, E.M. Rocher, C. Rödenbeck, U. Schuster, J. Swinger, R. Séferian, I. Skjelvan, T.
628 Steinhoff, A. Sutton, P. P. Tans, H. Tian, B. Tilbrook, F. N. Tubiello, I. T. vander Laan-Luijkx,
629 G. R. vander Werf, N. Viovy, A. P. Walker, A.J. Wiltshire, R. Wright, S. Zaehle, Bo. Zheng:
630 Global Carbon Budget 2018. *Earth Syst. Sci. Data.* 10, 2141–2194, <https://doi.org/10.5194/essd-10-2141-2018>, 2018

632 Levin, I., B., M. S. Kromer, H. Sartorius: A novel approach for independent budgeting of fossil
633 fuel CO₂ over Europe by ¹⁴CO₂ observations, *Geophys. Res. Lett.* 30(23), 2194,
634 doi:10.1029/2003GL018477, 2003

635 Li, S., J. Kim, S. Park, S.-K. Kim, M.-K. Park, J. Mühle, G.-W. Lee, M. Lee, C. O. Jo, K.-R.
636 Kim: Source identification and apportionment of halogenated compounds observed at a remote
637 site in East Asia. *Environ. Sci. Technol.* 48, 491–498, doi.org/10.1021/es402776w, 2014

638 Miller, J.B., S. J. Lehman, S. A. Montzka, C. Sweeney, B. R. Miller, A. Karion, C. Wolak, E. J.
639 Dlugokencky, J. Sounth, J. C. Turnbull, P.P. Tans: Linking emissions of fossil fuel CO₂ and
640 other anthropogenic trace gases using atmospheric ¹⁴CO₂. *J.Geophys.Res.* 117, D08302,
641 doi:10.1029/2011JD017048, 2012

642 Niu, Z., W. Zhou, X. Feng, T. Feng, S. Wu, P. Cheng, X. Lu, H. Du, X. Xiong, Y. Fu:
643 Atmospheric fossil fuel CO₂ traced by ¹⁴CO₂ and air quality index pollutant observations in

644 Beijing and Xiamen, China. *Environ. Sci. Pollut. Res.* 25, 17109–17117,
645 doi.org/10.1007/s11356-018-1616-z, **2018**

646 Niu, Z., W. Zhou, P. Cheng, S. Wu, X. Lu, X. Xiong, H. Du, Y. Fu: Observations of atmospheric
647 $\Delta^{14}\text{CO}_2$ at the global and regional background sites in China: Implication for fossil fuel CO_2
648 inputs. *Eviron. Sci. Technol.* 50, 12122–12128 DOI: 10.1021/acs.est.6b02814, **2016**

649 Nydal, R., and K. Lövseth, Carbon-14 measurements in atmospheric CO_2 from Northern and
650 Southern Hemisphere sites, 1962–1993, technical report, *Carbon Dioxide Inf. Anal. Cent., Oak*
651 *Ridge Natl. Lab.*, U.S. Dep. of Energy, Oak Ridge, Tenn, **1996**

652 Rafter, T. A., and G. J. Fergusson, “Atom Bomb Effect”—Recent increase of Carbon-14 content
653 of the atmosphere and biosphere, *Science*, 126(3273), 557–558, **1957**

654 Palstra, S. W., U. Karstens, H.-J. Streurman, H. A. J. Meijer: Wine ethanol ^{14}C as a tracer for
655 fossil fuel CO_2 emissions in Europe: Measurements and model comparison, *J. Geophys. Res.*,
656 113, D21305, doi:10.1029/2008JD010282, **2008**

657 Riley, W. G., D. Y. Hsueh, J. T. Randerson, M. L. Fischer, J. Hatch, D. E. Pataki, W. Wang, M.
658 L. Goulden: Where do fossil fuel carbon dioxide emissions from California go? An analysis
659 based on radiocarbon observations and an atmospheric transport model, *J. Geophys. Res.*, 113,
660 G04002, doi:10.1029/2007JG000625, **2008**

661 Rivier, L., P. Ciais, D. A. Hauglustaine, P. Bakwin, P. Bousquet, P. Peylin, A. Klonecki:
662 Evaluation of SF_6 , C_2Cl_4 , and CO to approximate fossil fuel CO_2 in the Northern Hemisphere
663 using a chemistry transport model. *J. Geophys. Res.* 111, D16311, doi:10.1029/2005JD006725,
664 **2006**

665 Suntharalingam, P., D. J. Jacob, P. I. Palmer, J. A. Logan, R.M. Yantosca, Y. Xiao, M. J. Evans:
666 Improved quantification of Chinese carbon fluxes using CO₂/CO correlations in Asian outflow, *J.*
667 *Geophys. Res.* 109, D18S18, doi:10.1029/2003JD004362, **2004**

668 Suess, H. E. Radiocarbon concentration in modern wood, *Science*, 122, 415, **1955**

669 Stuiver, M., P. Quay: Atmospheric ¹⁴C changes resulting from fossil fuel CO₂ release and cosmic
670 ray flux variability, *Earth Planet. Sci. Lett.* 53, 349–362, **1981**

671 Tang, W., A. F. Arellano, J. P. DiGangi, Y. Choi, G. S. Diskin, A. Agustí-Panareda, M.
672 Parrington, S. Massart, B. Gaubert, Y. Lee, D. Kim, J. Jung, J. Hong, J.-W. Hong, Y. Kanaya, M.
673 Lee, R. M. Stauffer, A. M. Thompson, J. H. Flynn, J.-H. Woo: Evaluating high-resolution
674 forecasts of atmospheric CO and CO₂ from a global prediction system during KORUS-AQ field
675 campaign. *Atmos. Chem. Phys.* 18, 11007–11030, doi.org/10.5194/acp-18-11007-2018, **2018**

676 Tans, P. P.; J. A. Berry, R. F. Keeling: Oceanic ¹³C/¹²C observations: A new window on ocean
677 CO₂ uptake. *Global Biogeochem. Cycles.* 7(2), 353–368, doi:10.1029/93GB00053, **1993**

678 Sokal, R. R., and F. J. Rohlf. 1981. Biometry. 2nd edition. Freeman, NY.

679 Song Jinming, Baoxiao Qu, Xuegang Li, Huamao Yuan, Ning Li, Liqin Duan: Carbon
680 sinks/sources in the Yellow and East China Seas-Air-sea interface exchange, dissolution in
681 seawater, and burial in sediments. *Science China Earth Sciences.* 61, 1583-1593, **2018**

682 Stuiver, M., Polach H. A. Discussion: Reporting of ¹⁴C data, *Radiocarbon*, 19(3), 355–363, **1977**

683 Tans, P.P., A.F.M. de Jong, W.G. Mook: Natural atmospheric ¹⁴C variation and the Suess effect,
684 *Science*, 280, 826-828, **1979**

685 Thoning, K. W., P. P. Tans, W. D. Komhyr: Atmospheric Carbon dioxide at Mauna Loa
686 Observatory 2. Analysis of the NOAA GMCC Data, 1984–1985, *J. Geophys. Res.* **94**, 8549–
687 8565, **1989**

688 Tohjima, Y., M. Kubo, C. Minejima, H. Mukai, H. Tanimoto, A. Ganshin, S. Maksyutov, K.
689 Katsumata, T. Machida, K. Kita: Temporal changes in the emissions of CH₄ and CO from China
690 estimated from CH₄/CO₂ and CO/CO₂ correlations observed at Hateruma Island. *Atmos. Chem.*
691 *Phys.* **14**, 1663–1677, doi:10.5194/acp-14-1663-2014, **2014**

692 Turnbull, J., P. Rayner, J. Miller, T. Naegler, P. Ciais, A. Cozic: On the use of ¹⁴CO₂ as a tracer
693 for fossil fuel CO₂: Quantifying uncertainties using an atmospheric transport model, *J. Geophys.*
694 *Res.* **114**, D22302, doi:10.1029/2009JD012308, **2009**

695 Turnbull, J. C., S. J. Lehman, J. B. Miller, R. J. Sparks, J. R. Sounth, P. P. Tans: A new high
696 precision ¹⁴CO₂ time series for North American continental air. *J. Geophys. Res.* **112**, D11310,
697 doi:10.1029/2006JD008184, **2007**

698 Turnbull, J. C., P. P. Tans, S. J. Lehman, D. Baker, T. J. Conway, Y. S. Chung, J. Gregg, J. B.
699 Miller, J. R. Sounth, L.-X. Zhou: Atmospheric observations of carbon monoxide and fossil fuel
700 CO₂ emissions from East Asia. *J. Geophys. Res.*, **116**, D24306, doi:10.1029/2011JD016691,
701 **2011a**

702 Turnbull, J. C., A. Karion, M. L. Fischer, I. Faloona, T. Guilderson, S. J. Lehman, B. R. Miller, J.
703 B. Miller, S. Montzka, T. Sherwood, S. Saripalli, C. Sweeney, P. P. Tans: Assessment of fossil
704 fuel carbon dioxide and other anthropogenic trace gas emissions from airborne measurements

705 over Sacramento, California in spring 2009, *Atmos. Chem. Phys.* 11(2), 705–721,
706 doi:10.5194/acp-11-705-2011, **2011b**

707 Turnbull, J. C. J. B. Miller, S. J. Lehman, P. P. Tans, R. J. Sparks, J. Sounthor: Comparison of
708 $^{14}\text{CO}_2$, CO, and SF₆ as tracers for recently added fossil fuel CO₂ in the atmosphere and
709 implications for biological CO₂ exchange, *Geophys. Res. Lett.*, 33, L01817,
710 doi:10.1029/2005GL024213, **2006**

711 Van Der Laan, S, U. Karstens, R.E.M . Neubert, I.T. Van Der Laan-Luijkx and H.A.J. Meijer:
712 Observation-based estimates of fossil fuel-derived CO₂ emissions in the Netherlands using $\Delta^{14}\text{C}$,
713 CO and $^{222}\text{Radon}$, *Tellus B: Chemical and Physical Meteorology*, 62:5, 389-402,
714 DOI:10.1111/j.1600-0889.2010.00493.x. **2010**

715 Wang, Y. J. W. Munger, S. Xu, M. B. McElroy, J. Hao, C. Nielsen, H. Ma: CO₂ and its
716 correlation with CO at a rural site near Beijing: Implications for combustion efficiency in China,
717 *Atmos. Chem. Phys.* 10, 8881–8897, doi:10.5194/acp-10-8881-2010, **2010**

718 Yin, L., P. Du, M. Zhang, M. Liu, T. Xu, Y. Song: Estimation of emissions from biomass
719 burning in China (2003–2017) based on MODIS fire radiative energy data, *Biogeosciences*, 16,
720 1629–1640. **2019**

721 Zondervan, A., and Meijer, H. A. J: Isotopic characterization of CO₂ sources during regional
722 pollution events using isotopic and radiocarbon analysis, *Tellus B: Chemical and Physical*
723 *Meteorology*, 48(4), 601–612, doi:10.1034/j.1600-0889.1996.00013.x, **1996**